Published in
Applied Physics B : Lasers and Optics 95, issue 4, 813-824, 2009
which should be used for any reference to this work

Performance evaluation of a near infrared QEPAS based ethylene sensor

S. Schilt · A.A. Kosterev · F.K. Tittel

Abstract A sensor based on quartz-enhanced photoacoustic spectroscopy (QEPAS) was evaluated for the detection of trace levels of ethylene at atmospheric pressure using a fiber coupled DFB diode laser emitting in the 1.62 μm spectral range. A noise-equivalent QEPAS signal of ∼4 ppm C_2H_4 was achieved for a 0.7 s data acquisition time using wavelength-modulation with a second-harmonic detection scheme on the strongest C_2H_4 absorption peak at 6177.14 cm^{-1} with an average optical power of ∼15 mW. Improved detection sensitivity of 0.5 and 0.3 ppm C_2H_4 (1σ) was demonstrated using longer averaging time of 70 and 700 s, respectively. Important characteristics for the QEPAS based sensor operation in real-world conditions are presented, particularly the influence of external temperature variations. Furthermore, the response time of the ethylene sensor was measured in different configurations and it is shown that the QEPAS technique can provide a response time in a few seconds range even without active gas flow.

1 Introduction

Quartz-enhanced photoacoustic spectroscopy (QEPAS) is a spectroscopic technique that combines the main characteristics of photoacoustic spectroscopy (PAS) with the benefits of a quartz tuning fork (QTF), providing an ultracompact, robust, and cost-effective trace gas sensing module. The QEPAS sensor is based on a high-Q quartz resonator mass-produced as a frequency reference for clocks and watches. The resonance frequency of readily commercially available QTFs is 32.8 kHz compared to the operation frequency of a few kHz in conventional PAS. This makes QEPAS sensors insensitive to ambient acoustic noise, which often limits PAS sensitivity. The reduction of the PAS signal associated with the high QTF resonance frequency (the PAS signal scales as $1/f$) is compensated by the high Q-factor of the QTF (from a $Q = 10^5$ in vacuum to $Q = \sim 10^4$ at atmospheric pressure) compared to PAS resonators with Q-factor ranging from a few tens for longitudinal resonances up to several hundreds for radial resonances. Hence, QEPAS can achieve a comparable sensitivity as conventional PAS but with important benefits, such as reduced size and ambient acoustic noise impact.

Since the discovery of QEPAS several years ago [1], it has been demonstrated with several simple molecules using a single rovibrational line in fundamental mid-IR absorption bands [2, 3] (e.g., CO, N_2O, H_2CO, C_2H_6) or in near-IR combination bands (e.g., NH_3 [4], CO_2 [5], HCN [6], H_2S [7]). More recently, QEPAS has also been implemented with larger molecules with broad, unresolved absorption spectra, such as acetone and freons [8–10]. The main difference in the implementation of QEPAS with narrow-line molecules and broadband absorbers is that wavelength modulation (WM) at half the QTF resonance frequency with second-harmonic ($2f$) detection and reduced pressure operation is applicable for target analytes with well-resolved absorption lines, whereas amplitude modulation (AM) at the QTF frequency and detection at the same frequency is necessary for molecular species with unresolved congested spectra.

S. Schilt (✉)
IR Microsystems SA, PSE-C, 1015 Lausanne, Switzerland
e-mail: schilt@ir-microsystems.com

A.A. Kosterev · F.K. Tittel
Electrical and Computer Engineering Department, Rice University, Houston, TX 77005, USA

In this work, we investigated the use of QEPAS for the detection and the quantification of ethylene (C_2H_4). This molecule represents the intermediate case between isolated narrow lines and broadband spectra previously detected with QEPAS. The C_2H_4 spectrum has a partially resolved rotational structure with a high density of lines that merge or overlap so that no isolated lines occur at atmospheric pressure. The use of QEPAS with WM and $2f$ detection was applied at atmospheric pressure conditions in order to fulfill the requirements for a potential application in the fruit transportation and storage industry and comparative AM-QEPAS measurements were performed.

Ethylene is a plant hormone that plays an essential role in regulating the growth, development, ripening, and decay of fruits and vegetables. This molecular species is emitted during the ripening process and furthermore acts as a catalyst to initiate or fasten the ripening and decaying processes so that the presence of even trace amounts of ethylene during the shipping and storage of fruits (from ppmv down to ppbv level depending on the fruit variety) causes a premature degradation of most fresh produce. Hence, the control of trace C_2H_4 concentrations during fruit transportation is essential to improve the quality of shipped fruit and to deliver the best possible products to consumers. For example, the typical required C_2H_4 detection sensitivity is $\sim$1 ppmv for the transport of bananas. The availability of a cost-effective ethylene sensor would offer a breakthrough for the fruit transportation and storage industry, since no cost-effective and suitable sensor technology is currently available. Current instrumentation does not achieve the necessary operating performance (e.g., stability, lifetime) or is too costly (e.g., gas chromatography). We therefore investigated the potential of QEPAS in conjunction with a cost-effective commercially available near-infrared DFB laser diode to develop a prototype C_2H_4 sensor with the objective to address this particular application. In this work, we mainly focus on an evaluation of the achievable performance in real-world conditions for the intended application. Therefore, of prime importance in this study was the sensor operation at atmospheric pressure as well as its temperature behavior, its use without forced air flow and the impact of potential interfering species.

2 QEPAS-based sensor description

The architecture of the ethylene sensor used in this work was described in previous publications [2, 6] and was applied to the detection of several gases, including CO_2, H_2O, H_2S, NH_3, CH_4, HCN, and C_2H_2 in the NIR spectral region. The current ethylene sensor schematic is shown in Fig. 1. The control electronics unit (CEU) incorporated a digital diode laser injection current driver and temperature controller. The

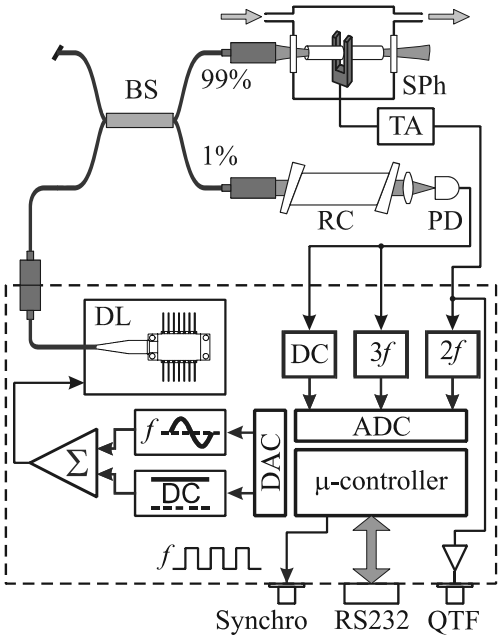

Fig. 1 Schematic of the QEPAS sensor used for trace ethylene detection. The *dashed box* outlines the elements inside the control electronics unit (CEU). BS—99:1 fiber beam splitter; SPh—spectrophone (tuning fork with microresonator); TA—transimpedance amplifier positioned close to the SPh; RC—reference gas cell filled with a mixture of 440 Torr C_2H_4 and 295 Torr N_2; PD—photodetector; DC, $3f$, and $2f$—analog front stages converting respectively DC, $3f$ and $2f$ components of the input signal into voltage; DL—diode laser with temperature controller and injection current driver. CEU connectors: "Synchro"—a rectangular 0 to +5 V wave at the laser modulation frequency f; "QTF"—amplified signal from the quartz tuning fork; RS232—communication port for remote control and data exchange

excitation DFB diode laser (NEL model NLK1556STB) with a single-mode fiber output is mounted on an electronics board inside the CEU. A WM-$2f$ spectroscopic approach is used. The DC component of the diode laser current ($\sim$130 mA) determines the laser power and wavelength at a given temperature, while a smaller AC component ($\sim$20 mA amplitude) results in WM at the frequency f. Detection of the QTF generated current is performed at the resonant QTF frequency $f_0 = 2f$, where $f_0 \approx 32.8$ kHz. The output radiation of the 1.62 μm diode laser is split in a 99:1 power ratio. This allows 1% of the optical power to be directed to a sealed reference gas cell (length 3 cm) filled with a specified 60% C_2H_4 concentration in N_2 at 740 Torr and subsequently to a photodetector (PD). The $3f$ component U_{3f} of the PD signal is used by the CEU for locking the laser to a selected peak of the ethylene absorption spectrum. The U_{3f} component is used as an error signal in the laser DC current feedback loop, because it resembles the 3rd derivative of the C_2H_4 absorption spectrum and has its zero-crossing point where the signal at $2f$ is at a maximum [11, 12]. The remaining 99% of the laser radiation ($\sim$15 mW average optical power for typical laser operating conditions) is directed

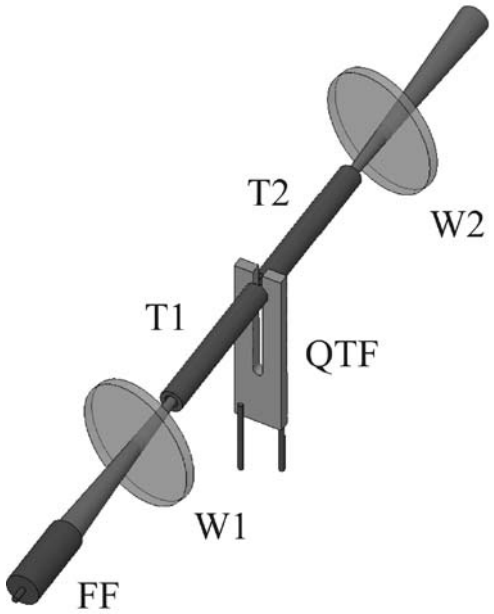

Fig. 2 The spectrophone design and optical configuration. FF—fiber focuser with 15 mm effective focal length; W1, W2—BK7 windows, AR coated for $\lambda = 1050$–1620 nm and tilted at $\sim 10°$ from the normal to the optical axis position to prevent reflected light reaching the spectrophone; T1, T2—5.1 mm long pieces of 0.41 mm inner diameter stainless steel hypodermic tubing, forming the acoustic microresonator; QTF—a quartz tuning fork (largest crystal dimension 6.23 mm). The gas cell enclosing the spectrophone and that holds W1, W2 is not shown

to the spectrophone (SPh) consisting of a QTF and an organ pipe type of acoustic microresonator (μR), as depicted in Fig. 2. The total length of each of the two μR tubes is 5.1 mm (close to $\lambda/2$ for a sound wave of 32.8 kHz in air or N_2). This is approximately twice longer than have been used in earlier sensor versions [2, 3] and was experimentally found to produce higher photoacoustic signals at >500 Torr gas pressure. The gaps between each of the μR tubes and a QTF surface were in the 30–50 μm range. The enhancement factor provided by the μR amounts to ∼15 in this geometry. A GRIN-lens-based fiber-coupled focuser with 15 mm effective focal length is used to direct the laser radiation through 0.41 mm diameter μR tubes. Micropositioners were used to precisely align the laser beam through the spectrophone. The spectrophone was located in a compact cell described earlier in [4] with ~ 1 cm^3 volume. The positioner/focuser assembly together with the spectrophone cell constitutes the sensing module. The electrical response of the QTF to the laser induced acoustic wave is detected using a transimpedance amplifier (TA) with a $R_{FB} = 10$ MΩ feedback resistor.

Functions performed by the CEU incorporating the laser current and temperature controller include:

- Determination of the electromechanical parameters of the QTF: its dynamic resistance R, quality factor Q, and resonant frequency f_0;
- Setting of the laser modulation frequency to $f = f_0/2$;
- Measuring and digitizing the input signals: $2f$ component of the QTF signal, $3f$ and DC components of the PD signal;
- Auto-calibrating "0" signal levels (which can drift because of the analog front end) by detuning the laser from the locked-to-the-line optical frequency to absorption-free frequency and measuring the corresponding $2f$ component of the QTF signal;
- Sending digitized data to a computer via RS232 port and receiving remote commands such as follows: set diode laser current or temperature to a certain value; change the laser current modulation index; measure the QTF parameters and lock the laser wavelength to the absorption line.

The internal lock-in detector for QTF signal measurements has an equivalent noise bandwidth of $\Delta f = 0.785$ Hz. Digitized results are updated on the CEU display and the RS232 port every 0.7 s. The in-phase signal value is expressed in the analog-to-digital converter (ADC) counts (cnt); 1 cnt = 1.8 nV rms voltage at the QTF transimpedance preamplifier output, or 1.8×10^{-16} A rms current generated by the QTF.

A PC computer with LabView-based software is used for controlling the CEU operation, as well as receiving and logging the data. The CEU is capable of autonomous operation (without PC) and internal data logging, but this function was not used in the present work. The CEU is also equipped with an amplified QTF signal output (×30 of the TA signal) and synchronization signal at frequency f, which enabled the monitoring of the QTF signal on an oscilloscope or to use an external lock-in amplifier. These functions are especially useful during the initial sensor setup procedures to ensure proper grounding, electromagnetic shielding, and optimum settings of the phase of internal CEU lock-in amplifiers.

2.1 Spectral calibration and C_2H_4 absorption line selection

For precise calibration of the diode laser wavelength as a function of its temperature and current, we initially scan the laser temperature at a fixed DC current $I_l = 130$ mA (no modulation) and record the PD signal after the reference cell. The baseline is approximated by a smooth fit of transmitted power vs. the laser temperature, and thus an approximate absorption spectrum is derived. This absorption spectrum is then compared to the FTIR spectrum from the PNNL database [13]. The corresponding C_2H_4 absorption peaks can be readily identified (Fig. 3). The calibration yields a -0.44 cm^{-1}/°C diode laser thermal tuning coefficient.

A set of $2f$ absorption spectra is then acquired using the same reference cell with different laser current modulation amplitudes A_I corresponding to wavelength modulation amplitudes A_{WL}. The acquired spectra are compared to

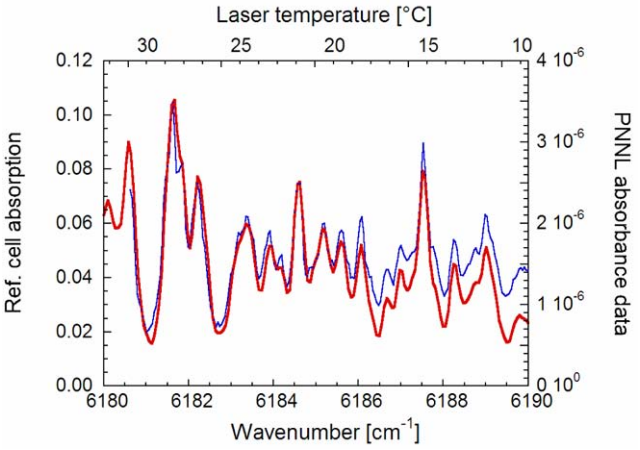

Fig. 3 Ethylene absorption spectrum from PNNL database (*thick line*) and experimentally observed from the reference cell when scanning the diode laser temperature (*thin line with dots*)

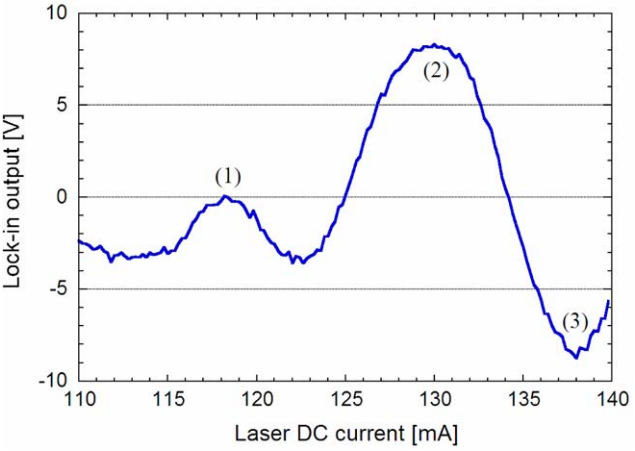

Fig. 5 QEPAS spectrum of a 101 ppmv C_2H_4:N_2 calibrated gas mixture acquired at a 6177.14 cm^{-1} peak by means of diode laser current scanning

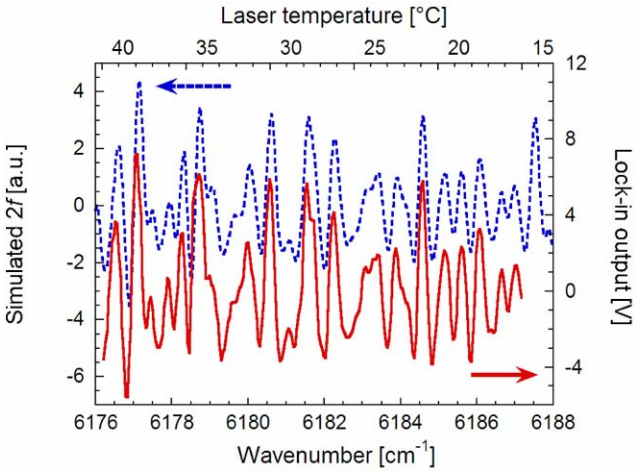

Fig. 4 $2f$ absorption spectra of ethylene: simulated with $A_{WL} = 0.22$ cm^{-1} (*solid line*) and experimental with $A_I = 20$ mA and $I_l = 130$ mA laser current (*dashed line*)

the numerically simulated $2f$ spectra based on PNNL database values. Based on a spectral comparison, such as shown in Fig. 4, it was established that the optimum current modulation $A_I = 20$ mA results in $A_{WL} = 0.22$ cm^{-1}. Both the simulated and experimental $2f$ absorption spectra show that the highest peak is located at 6177.14 cm^{-1} and accessed at the diode laser temperature of +37.95°C and $I_l = 130$ mA. This peak is free from strong interference of common air constituents, such as H_2O and CO_2 (more details and experimental proof are presented in Sect. 3.2). Therefore, this particular peak was selected for ethylene monitoring.

A high-resolution QEPAS spectrum of a 101 ppmv C_2H_4:N_2 calibrated mixture obtained by varying the diode laser current I_l at a fixed temperature of +37.95°C is shown in Fig. 5. The QEPAS signal is detected using an external lock-in amplifier as described above (time constant $\tau = 1$ s, 12 dB/oct low-pass filter, 2 mV rms range). The selected peak (2) is located at $I_l = 130.0$ mA, as expected. The plot reveals two more advantages of using this particular spectral feature. First, a smaller peak (1) at $I_l = 118.2$ mA (6177.49 cm^{-1}) has a signal equal to zero (which can be achieved by adjusting A_I and, hence, A_{WL}). Therefore, the selected optimum C_2H_4 absorption line allows calibrating both $2f$ and $3f$ zero levels of the CEU electronics by tuning the laser current to 118.2 mA. Second, a negative peak (3) at 138.0 mA (6176.90 cm^{-1}) is almost as strong as the positive target peak (2). Therefore, for better zero level drift compensation, the laser can be alternately tuned to either the peak at 6177.14 cm^{-1} or the valley at 6176.90 cm^{-1} with the C_2H_4 concentration being subsequently derived from the difference of the measured signals. Thus, zero drifts can be cancelled without sacrificing data acquisition time by performing the measurements in the zero-signal spectral regions.

3 Performance of the QEPAS-based ethylene sensor

3.1 Calibration and detection sensitivity characteristics

The sensor response to varying C_2H_4 concentration levels in N_2 is displayed in Fig. 6. Different C_2H_4 concentrations in the 0–100 ppmv range were generated by diluting the 100 ppmv C_2H_4:N_2 calibrated gas mixture using a sonic nozzles gas mixer. Supplying pure N_2 to the sensor reveals an offset of the zero level related primarily to limitations of the CEU version used in this work (internal cross-talk between the laser modulation and the signal detection circuits). A minor contribution of stray radiation absorbed in the spectrophone may also be present. When the measured zero level offset was subtracted, an excellent linearity of the

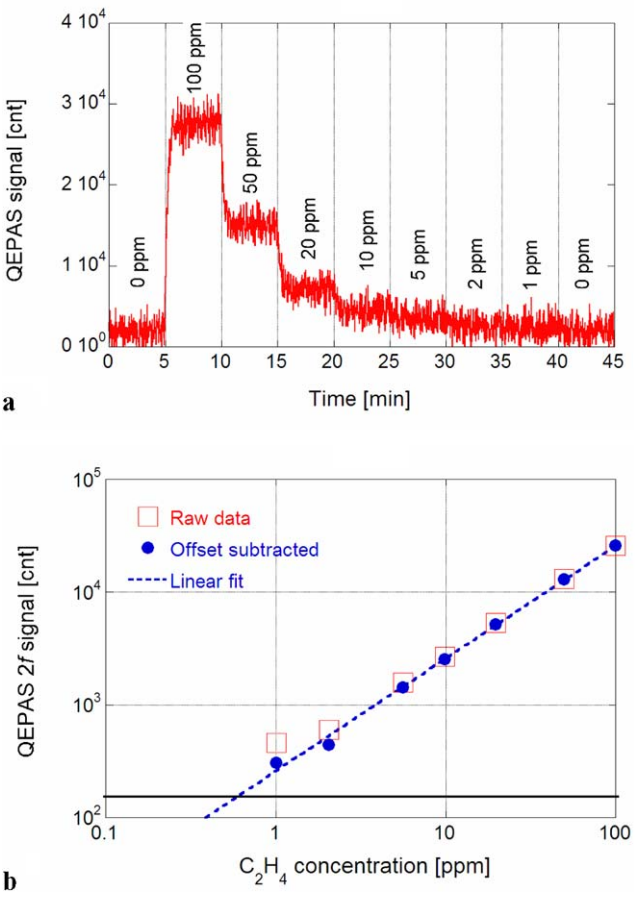

Fig. 6 **a** Response of QEPAS sensor to C_2H_4 concentration steps for 0.7 s data acquisition time. **b** Corresponding calibration curve obtained by averaging data over three minutes for each concentration step displayed in (**a**) and subtracting the measured zero concentration offset indicated by the *black horizontal line*. The detected signal is expressed in the CEU ADC counts (cnt)

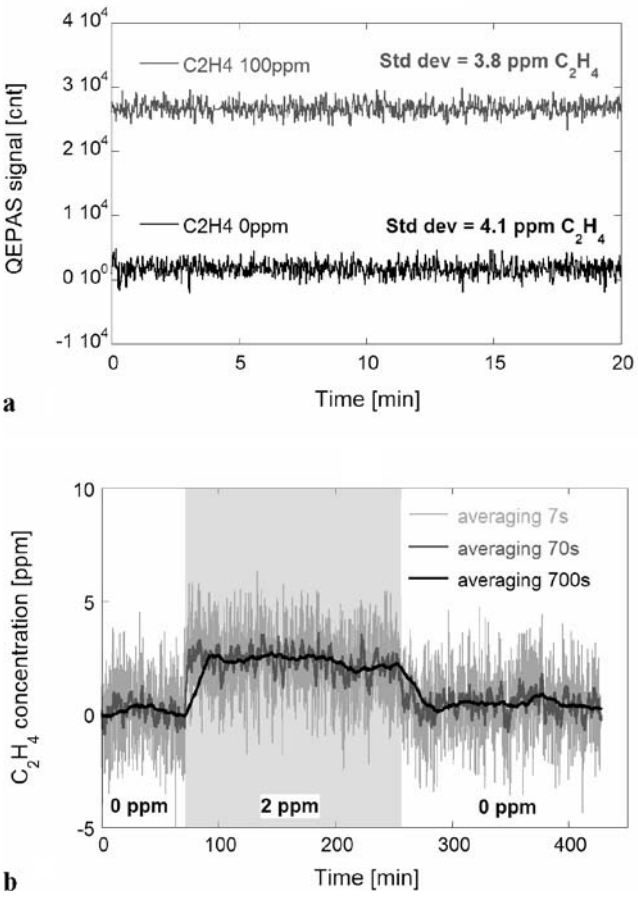

Fig. 7 **a** Short-term noise of the QEPAS signal measured over 20 min period for 100 and 0 ppmv C_2H_4 (averaging time 0.7 s). **b** 0–2 ppmv C_2H_4 step observed at different averaging times

QEPAS signal versus C_2H_4 concentration is achieved. A linear fit shown in Fig. 6b yields a calibration coefficient of 3.9×10^{-3} ppmv per 1 cnt, or 21.5 ppmv per 1 pA rms of the QTF generated current.

With a sampling interval of 0.7 s (one event of the CEU digital output, no additional averaging), rms noise (1σ) derived from a 20 min run is 1020 cnt = 1.8 μV rms. This value is in agreement with the theoretically calculated thermal noise of the QTF at this pressure and room temperature. Thermal noise in one of the two quadrature components is given by the equation (see [2] and references therein):

$$N_{th} = \frac{1}{\sqrt{2}} R_{FB} \sqrt{\frac{4k_B T}{R}} \sqrt{\Delta f} \tag{1}$$

The QTF dynamic resistance in the spectrophone module was measured to be $R = 198$ kΩ at atmospheric pressure, and the CEU bandwidth was $\Delta f = 0.785$ Hz as mentioned in Sect. 2. This noise level does not depend on the C_2H_4 concentration and corresponds to ∼4 ppmv C_2H_4 as shown in Fig. 7a, verified with both a 100 ppmv C_2H_4 concentration and zero-air. With a 0.7 s integration time, a concentration step of ∼10 ppmv C_2H_4 is visible, while smaller steps are difficult to distinguish. Longer averaging times allow detecting smaller concentration changes. Figure 7b displays a 2 ppmv step measured with three different data acquisition averaging times. This C_2H_4 concentration level becomes clearly visible with averaging times ranging from 70 to 700 s, for which the short-term noise (1σ) is respectively improved to 0.5 and 0.3 ppmv C_2H_4. Such averaging times are compatible with the intended fruit transportation application, where a gas concentration information updated every 10–20 min is acceptable.

3.2 Spectral interference

The effect of potential interfering molecular species in the monitoring of C_2H_4 for fruit transportation and storage applications was also investigated. The main potential interferent is carbon dioxide (CO_2), which may be present up to several percent in the targeted application and which has weak lines belonging to the (0 0 0) → (1 4^0 1) and

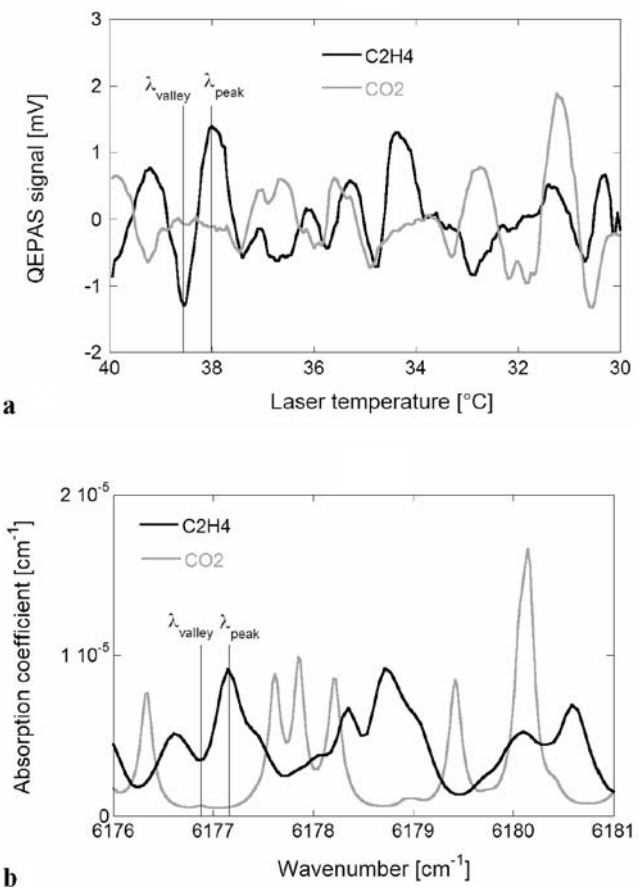

Fig. 8 **a** Experimental $2f$ QEPAS signals measured for 100 ppmv C_2H_4 and 13.9% CO_2. **b** Corresponding reference absorption spectra. The position of the considered C_2H_4 peak wavelength is indicated by λ_{peak}

$(0\ 1\ 0) \rightarrow (1\ 5^1\ 1)$ vibrational transitions in the diode laser operating spectral range. Measured QEPAS spectra of C_2H_4 (100 ppmv) and CO_2 (13.9%) are shown in Fig. 8 and are compared with reference absorption spectra computed from Hitran [14] (for CO_2) and PNNL [13] (for C_2H_4) databases. From this figure, the CO_2 contribution at the target position used for the measurement of C_2H_4 is expected to be minor (both for the peak and valley wavelengths). This was confirmed by monitoring the interference QEPAS signal at the C_2H_4 peak wavelength for various CO_2 concentrations. No influence is observed up to 9% CO_2 as shown in Fig. 9.

A second potential interferent is water vapor. The influence of humidity on the monitoring of C_2H_4 is shown in Fig. 10 in the case of 100 and 0 ppmv C_2H_4. The gas mixture was moisturized by passing the gas flow through a humidifier, i.e., a cuvette filled with liquid water at ambient temperature ($T = 20°C$). The flow exiting the humidifier was saturated in water vapor, corresponding to ~2.3% absolute H_2O concentration. For 100 ppmv C_2H_4, no difference in the QEPAS signal obtained in both dry and humid gas is observed. This demonstrates that a fast vibration-to-translation

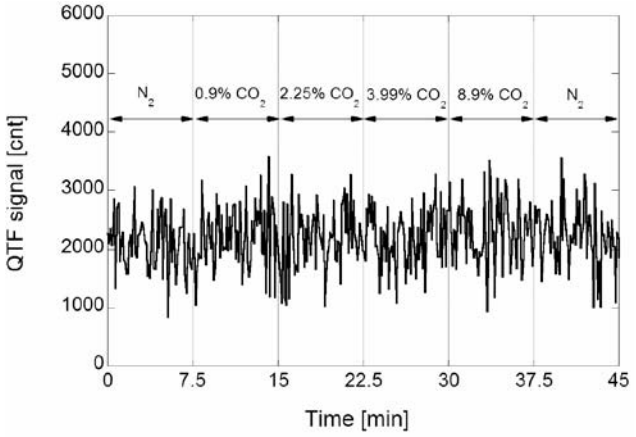

Fig. 9 Interference QEPAS signal at the C_2H_4 peak wavelength measured for different CO_2 concentrations (averaging time 7 s)

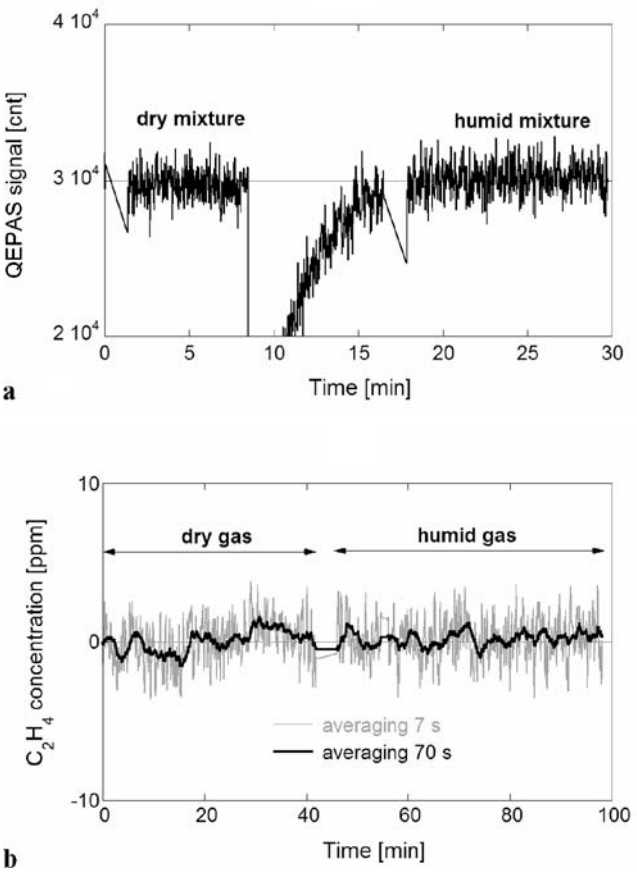

Fig. 10 **a** Influence of humidity on the QEPAS signal corresponding to 100 ppmv C_2H_4. The initial drop of the signal observed when the gas flow is passed through a humidifier ($t \sim 8$ min) results from a dilution of the C_2H_4 mixture since the humidifier was initially filled with dry air. **b** Comparison of the sensor zero (0 ppmv C_2H_4) in dry and humid N_2, showing no H_2O interference

relaxation occurs from the C_2H_4 excited state even in dry N_2, so that relaxation effects that have been reported for some conditions in PAS [15–17] and which are also relevant

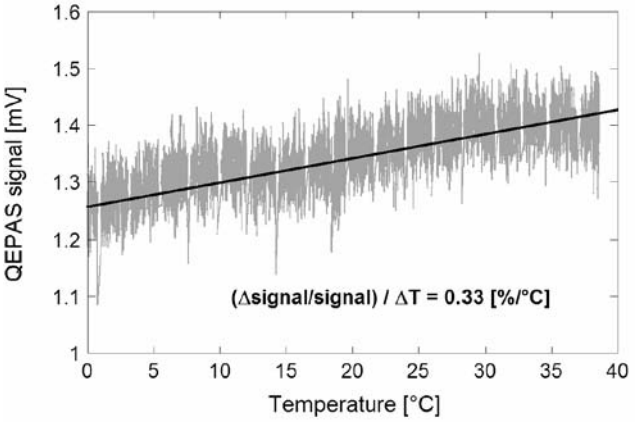

Fig. 11 Temperature-dependence of the QEPAS signal corresponding to 100 ppmv C_2H_4 observed during a slow (0.2°C/min) decreasing temperature ramp performed in a climate chamber. Measurement performed with an external lock-in amplifier with a 1 s time constant

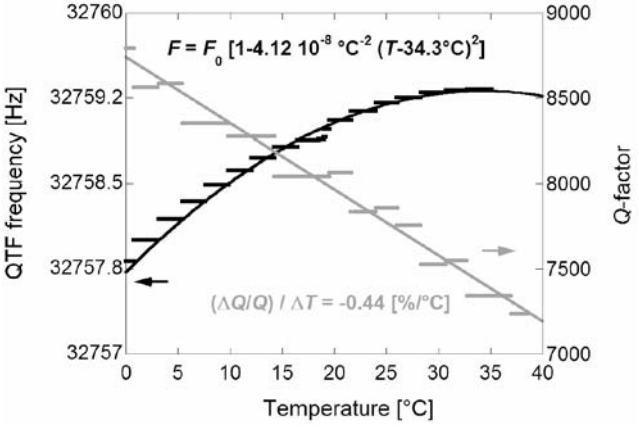

Fig. 12 Temperature-dependence of the QTF Q-factor and resonance frequency measured over a 40°C range

in QEPAS [5, 6, 18] due to the high operating frequency are not an issue in the case of C_2H_4. The comparison of the zero signal obtained in dry and humid (saturated at ambient temperature) nitrogen depicted in Fig. 10b shows the absence of an H_2O interference.

3.3 Thermal effects

The temperature behavior of the sensor has been investigated over a 40°C temperature range by inserting the sensing module (spectrophone, fiber-coupled focuser, optomechanical mounts, and transimpedance preamplifier) in a computer-controlled climate chamber and applying slow temperature ramps (typical 0.1–0.2°C/min). For these measurements the electronic modules (CEU and optional external lock-in) were located outside the chamber in order to investigate only the temperature effect on the optical QEPAS module. In order to maintain the modulation frequency on the QTF resonance during the entire test period, the resonance frequency (and the Q-factor) was determined every 10 min as mentioned in Sect. 2 and the diode laser modulation frequency was adjusted accordingly. Since the auto-calibration process is accompanied by an adjustment of the signal offset in the CEU, data from an external lock-in amplifier is generally used here, in order to avoid unwanted zero level changes that may occur in the CEU as a result of the auto-calibration process.

Figure 11 displays the temperature-dependant variation of the QEPAS signal corresponding to 100 ppmv C_2H_4. The observed slope of $\sim$0.33%/°C is mainly due to the temperature dependence of the C_2H_4 absorption at the target wavelength. No reference data has been found in the literature to compare the observed dependence. Additionally, there is a small contribution of the temperature dependence of the Q-factor (see below). No decrease of the QEPAS signal resulting from a possible temperature-dependent mismatch between the resonances of the QTF and the microresonator is noted in the entire investigated temperature range. We calculated that a $\sim$35% drop of the enhancement factor of the microresonator can be expected for a $\pm$20°C temperature change at room temperature based on calculations made for a standard longitudinal resonator with a 32.8 kHz central frequency and a $Q_{\mu R} = 15$ quality factor (drop due to the $T^{1/2}$ shift of the resonance). The experimental observations seem to indicate that the microresonator does not act as a classical acoustic resonator in PAS and its operation is more complex.

The temperature dependence of the QTF frequency and Q-factor observed in the tests is shown in Fig. 12. The frequency versus temperature curve is quadratic with a coefficient $\Delta F/\Delta T^2 = -0.04 \times 10^{-6}$ Hz/°C^2 which is similar to the one in vacuum. However, the parabolic maximum is shifted from its design position of $T_0 = 25$°C in vacuum to $T_0 = \sim$35°C at atmospheric pressure. The overall measured frequency variation over the 40°C temperature range is only 2 Hz, but this value is comparable to the half width at half maximum of the QTF resonance so that a continuous adjustment of the frequency is required in real application conditions to compensate the resonance drift induced by temperature fluctuations. In the considered temperature range, the Q-factor scales linearly with temperature, with a measured coefficient $(\Delta Q/Q)/\Delta T = -0.4\%$/°C.

The temperature stability of the zero level QEPAS signal was also measured during several successive temperature cycles made for slow ramps of 20°C temperature variation (over 3.5 h) separated by a 2.5 h plateau at 0, 20, and 40°C, respectively, as shown in Fig. 13 (measurement of the CEU $2f$ signal). Even if the QEPAS $2f$ signal appears to be quite stable over the entire measurement period when considering a short integration time of 0.7 s (besides some small areas with higher noise levels that is discussed below), a

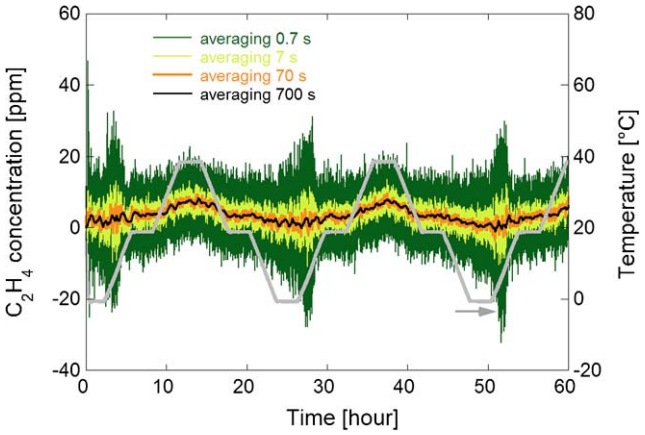

Fig. 13 Stability of the zero QEPAS signal for varying external temperatures observed for different averaging times. The temperature profile during this measurement is displayed on the right scale of the graph

slow drift of the signal correlated with the temperature variation appeared when longer averaging times were considered. A residual drift equivalent to 6–8 ppmv C_2H_4 occurred over the entire temperature range, which is in one order of magnitude larger than the short-term noise obtained for averaging times ranging from 70 to 700 s ($1\sigma = 0.5$–0.3 ppmv). This drift occurred despite the auto-calibration process that was performed every 10 min in order to adjust the modulation frequency and which should compensate the drift of the zero level by the means of the zero calibration phase. A similar drift was also observed when measuring the QTF signal with an external lock-in.

The slightly higher noise that is observed in every cycle at the end of the low-temperature plateau (0°C), when the temperature starts to increase, is believed to be related to water condensation on some parts of the optical module (probably the QTF preamplifier) when the temperature in the chamber starts to increase (more moisturized air flows in the chamber when the temperature increases, which can cause condensation on some cold parts).

The observed temperature-related drift of the zero level is believed to be associated to a combination of stray-radiation-induced background (wall noise) in the spectrophone and electronic pick-up noise, even if no significant wall noise and pick-up contributions were previously observed at $2f$ during the alignment of the sensor system (using a short averaging time). This was confirmed by additional experiments performed during a similar temperature cycle to separate these two effects. The wall noise contribution was investigated by comparing measurements performed with the fiber collimator connected to or disconnected from the diode laser, whereas the importance of pick-up noise was characterized by varying the laser modulation amplitude (with the fiber collimator disconnected from the laser). Both effects contribute to the observed zero-drift. This drift is a critical issue for long-term operation of the sensor at low C_2H_4 levels. It represents the main practical limitation of the sensor, rather than the short-term noise that is reduced using longer signal averaging. This drift issue can be minimized by measuring the QEPAS signals alternatively at two different wavelengths as indicated in Fig. 5 and discussed in Sect. 2.1. The difference of these signals will be a measure of the C_2H_4 concentration. This difference may be more stable with changing the temperature conditions than the peak absorption value. The reported evaluation was performed with a laboratory version of the optical absorption module, where commercial micropositioners were used to precisely align the laser beam into the microresonator. Such an arrangement is sensitive to a temperature-induced mechanical misalignment that contributes to the zero-drift by generating wall noise in the microresonator. A much improved temperature stability can be realized using a more compact configuration free of moving parts, in which a fiber collimator is mounted close to the microresonator, as well as an improved CEU to reduce electronics-related drifts.

3.4 Response time

In view of the potential application of the sensor for ethylene monitoring in the fruit transportation industry, its use in a diffusive mode of operation (i.e., without forced gas flow) was investigated in order to make the sensor architecture as simple as possible. A critical parameter in this case is the gas exchange time, which was determined for different configurations of the spectrophone cell with different size apertures limiting the gas exchange between the cell and the surroundings. A first example is shown in Fig. 14a for a configuration with a 9 mm diameter aperture on each side of the spectrophone cell. A second example is displayed in Fig. 14b of a fully exposed spectrophone (the cell has been removed) in order to assess its intrinsic response time without restrictions imposed by external elements. In the first measurement, the cell was filled with a 100 ppmv C_2H_4:N_2 mixture by passing the gas through one of the openings. When a stable QEPAS signal was obtained, the flow was interrupted and the apertures were released in order to enable gas diffusion from the cell. In a second experiment (Fig. 14b), the spectrophone was exposed to a flow of the same calibrated 100 ppmv C_2H_4:N_2 gas mixture. When a stable QEPAS signal was achieved, the gas flow was abruptly removed from the QTF and the signal decay was recorded using the external lock-in amplifier with 100 ms time constant. In each case, the signal was recorded as a function of time. The observed signal decay can be closely approximated by a biexponential function. In the cell configuration with two apertures, a fast decay component corresponds to a time constant $\tau_1 \sim 7.5$ s, whereas the second (τ_2) is ~10 times longer. As a result, an overall response time $t_{10} \sim 35$ s is achieved (t_{10} defined as the time needed to reach 10% of the initial signal). For the

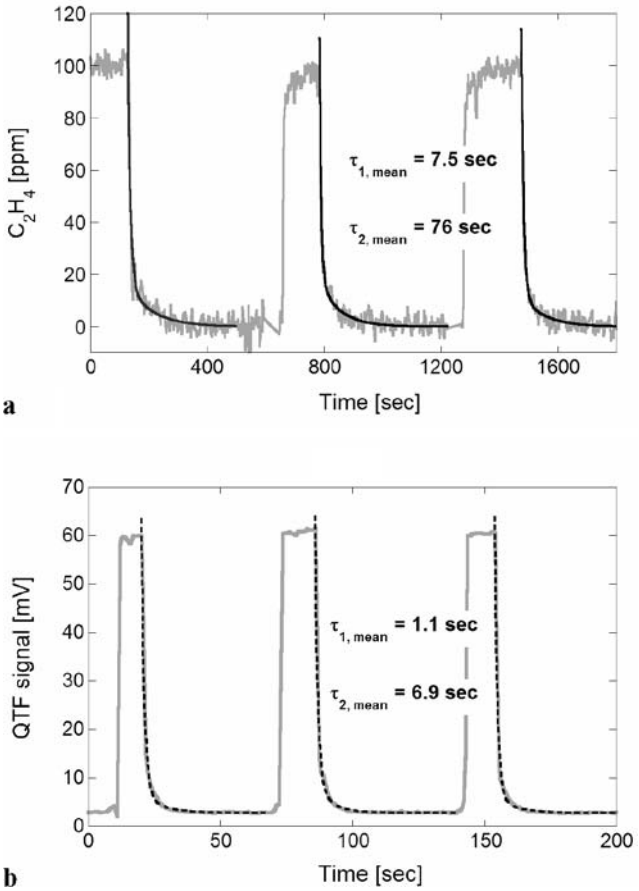

Fig. 14 Decay of the C_2H_4 QEPAS signal obtained in a diffusive operation mode with a ∅9 mm aperture on both sides of the spectrophone cell (**a**) and for a fully opened spectrophone (**b**)

open spectrophone, the faster decay component is reduced to $\tau_1 \sim 1.1$ s whereas the second is ∼6 times longer. A fast response time of $t_{10} \sim 4.5$ s is thus achieved, demonstrating that the QEPAS technique is capable of a response time of a few seconds even without active gas flow.

The observed biexponential behavior can be understood in terms of the concentration distribution in the microresonator. This distribution is described by an infinite sum of exponential decaying terms in the case of a tube initially filled with a gas which then diffuses to the outside through the two ends openings, as previously reported for similar conditions encountered with gas-filled hollow-core photonic band gap fibers [19, 20].

3.5 Comparison of WM-2f and AM-1f detection schemes

The behavior of the QEPAS sensor operating in either WM-2f or AM-1f modes was compared. In order to allow an easy interchange between these two operation modes, the diode laser was operated with a commercial diode laser driver (ILX-3782B) and its current was modulated using a

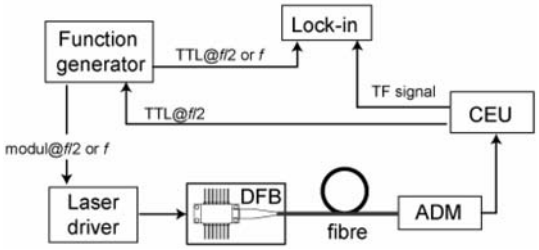

Fig. 15 Schematics of the experimental setup used to compare QEPAS with AM-1f and WM-2f modes

function generator synchronized to the reference frequency f_{ref} delivered by the CEU and equal to half the QTF resonance f_0 as depicted in Fig. 15. A diode laser current modulation at $f = f_{\mathrm{ref}} = f_0/2$ and lock-in demodulation at $2f = f_0$ was implemented for WM-2f, whereas a laser current modulation at $f = 2f_{\mathrm{ref}} = f_0$ and lock-in demodulation at $f = f_0$ was implemented for AM-1f. The modulation amplitude was optimized for the WM-2f mode of operation in order to maximize the C_2H_4 QEPAS signal, whereas a 100% modulation (from threshold up to the maximum current) was applied for the AM-1f detection scheme. The measured QEPAS spectra are displayed in Fig. 16 and are compared with a reference spectrum from the PNNL database [13]. A 1000 ppmv C_2H_4 concentration was used to provide an absorption signal well above the background level (in particular, in the case of AM-1f where a strong background signal is present). As expected, the AM-1f spectrum is a direct measurement of the C_2H_4 absorption coefficient and is similar to the reference spectrum, whereas the WM-2f signal is the second derivative of the absorption spectrum [21]. The spectral resolution of the AM-1f spectrum is slightly reduced due to the DFB diode laser wavelength chirp when its current is modulated.

Different waveforms (sine, square) were compared with the same average current level. For AM-1f, the square waveform modulation (50% duty cycle) generally produced a ∼25% higher signal than a sine modulation at the same average power level. This is in agreement with the difference in Fourier components at frequency $f = f_0$. In fact, the Fourier component of the laser power with symmetric rectangular modulation is $4/\pi\, P \cos(2\pi f_0 t)$, 27% higher than $P\cos(2\pi f_0 t)$ that a cosine wave modulation produces, where P is the average optical power. In case of WM-2f, signals of similar amplitude were obtained for both waveforms. The AM-1f signal was stronger by a factor ∼3 than the signal obtained by WM-2f for optimum modulation amplitude. This effect is mostly due to the nonstructured portion of the absorption spectrum, which does not contribute to the WM-2f signal. The QEPAS sensitivity demonstrated for C_2H_4 in the WM-2f mode can thus potentially be improved by this factor if an AM-1f approach is used. This is confirmed by the results of short-term stability

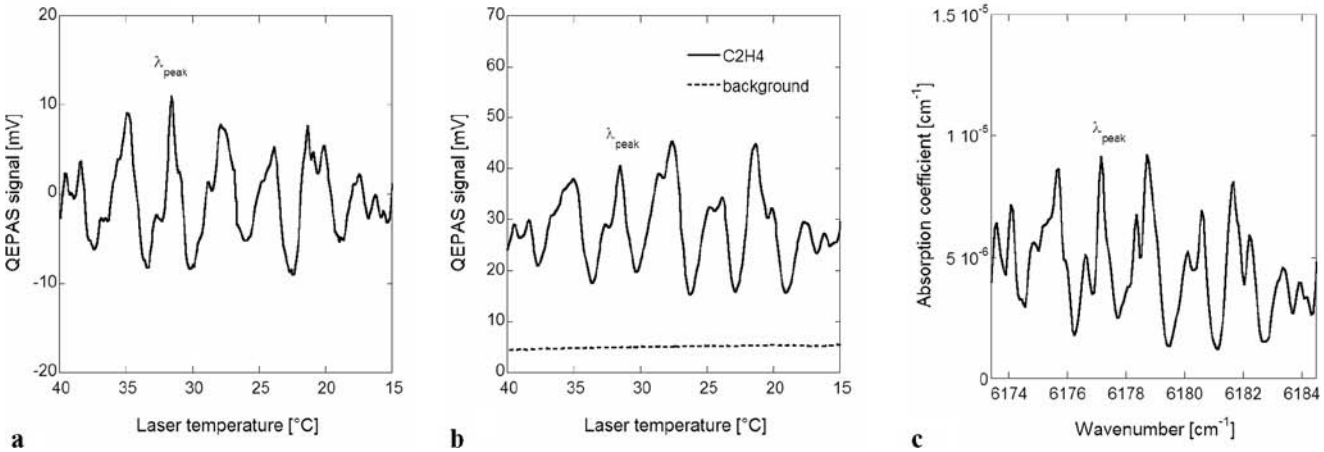

Fig. 16 C_2H_4 QEPAS spectra obtained for 1000 ppmv with WM-2f (**a**) and AM-1f (**b**) modes; comparison with a reference absorption spectrum (**c**)

Table 1 Comparison of contributions to the QEPAS signal measured for various modulation schemes and corresponding detection sensitivity. An external lock-in amplifier with a 1 s integration time was used

	AM-1f scheme				WM-2f scheme			
	Square modulation		Sine modulation		Square modulation		Sine modulation	
QTF signal	Mean	Std dev	Mean	Std dev	Mmean	Std dev	Mean	Std dev
C_2H_4 100 ppm [mV]	8.40	0.043	6.29	0.033	1.34	0.034	1.39	0.031
Background (air) [mV]	4.89	0.045	3.52	0.034	0.06	0.031	0.14	0.030
Pick-up (wo fibre) [mV]	0.63	0.047	0.12	0.032				
Calibr factor [μV/ppm]	35.1		27.7		12.77		12.5	
Noise eq signal [ppm]		1.25		1.20		2.63		2.47
Background [ppm C_2H_4]	139.2		126.7		4.9		11.2	
Pick-up noise [ppm C_2H_4]	17.8		4.2		0		0	

measurements performed for 100 and 0 ppmv C_2H_4 over a 10 min timescale for the different modulation schemes and waveforms, which are summarized in Table 1. The short-term noise was similar in all of the tested configurations ($1\sigma = \sim 30$ μV for a 1 s lock-in integration time) except for WM-1f with a square modulation where the noise was slightly stronger. Since the C_2H_4 QEPAS signal is typically 2 to 3 times stronger with AM-1f than with WM-2f, a better sensitivity is achieved with AM-1f. However, a strong background signal was observed for AM-1f with both square and sine modulations, as depicted in Fig. 16b. This background is equivalent to a 100 ppmv of C_2H_4 as a result of wall noise since it strongly decreased when the fiber collimator was disconnected from the ADM. An electronic pick-up contribution was also observed for AM-1f using a square waveform modulation, whereas this contribution disappeared with a smoother sine modulation. The residual background signal including both the wall noise and the pick-up noise was negligible for WM-2f, as previously mentioned, which represents a significant advantage of this modulation scheme.

The strong 1f background signal most likely originates from the stray light ending up on the walls of the microresonator and the QTF. This is confirmed by the observation that the amplitude of this offset strongly increases with a slight misalignment of the diode laser beam in lateral directions so that the beam wings touch the microresonator walls. The cell used in these experiments was not optimized to minimize internal scattering. The 1f-AM background level can be significantly reduced if careful consideration is given to the gas cell design.

In the AM-1f mode, not only the background offset value is large, but its temperature-dependant variations are higher than in the WM-2f mode: a drift of the sensor zero corresponding to hundreds of ppmv of C_2H_4 has been observed over a 40°C temperature range. A second measurement performed in the absence of wall noise (laser disconnected from the cell) has confirmed that these background fluctuations resulted from a wall noise, probably due

to small displacements of the laser beam in the microresonator induced by temperature variations. Significant improvements are expected when using a more stable collimator arrangement as well as by using larger diameter microresonator tubes.

4 Discussion and conclusions

A quartz-enhanced photoacoustic spectroscopy (QEPAS) sensor prototype was developed for C_2H_4 monitoring using a near-infrared (NIR) DFB laser emitting in the 1.62 μm wavelength range. The sensor was developed and characterized for a specific application, namely the monitoring of C_2H_4 for fruits transport and storage industry, where, for example, a sensitivity in the ppm range is required to be known for the transportation of bananas. To simplify as much as possible the sensor architecture atmospheric pressure operation was adopted. In this case, a noise-equivalent concentration of ∼4 ppm C_2H_4 was achieved for a 0.7 s data acquisition time using a WM-2f detection scheme on the strongest C_2H_4 absorption peak at 6177.14 cm^{-1} and using an average optical power of ∼15 mW. This detection limit corresponds to the thermal noise of the QTF at ambient temperature and pressure. This noise can be further reduced by using longer averaging times resulting in improved sensor sensitivities. Short-term noise of 0.5 and 0.3 ppm C_2H_4 (1σ) was thus achieved using an integration time of 70 and 700 s, respectively.

The sensor has also proven its insensitivity to the presence of potential interfering species such as carbon dioxide and water vapor, which can be present at high concentrations in the targeted application. No measurable interfering signal was observed for concentrations as high as 9% CO_2 and 2.3% H_2O (100% relative humidity at ambient temperature). The presence of water vapor has also shown no influence on the C_2H_4 QEPAS signal, demonstrating that C_2H_4 QEPAS measurements are not affected by relaxation effects.

The thermal behavior of the sensor was also investigated. Despite the experimentally observed temperature dependence of the spectrophone quality factor (−0.4%/°C), the C_2H_4 QEPAS signal showed a positive temperature dependence of 0.33%/°C, which is believed to mainly result from the temperature dependence of the linestrength of the C_2H_4 absorption line. A fundamental property for the application of the QEPAS sensor in real-world operating conditions was assessed from these thermal investigations, which is the absence of a decrease of the QEPAS signal resulting from a potential temperature-dependent mismatch between the QTF resonance and the microresonator, whereas such a drop would be expected for a standard longitudinal acoustic resonator. These observations seem to indicate that the microresonator does not act as a classical acoustic resonator in PAS. Additionally, a small drift of the zero level of the sensor was observed for varying external temperature conditions. This drift resulting from a combination of stray-radiation-induced wall noise and electronic pick-up noise currently limits the performance of the sensor to 6–8 ppm over a 40°C temperature range. An improved CEU as well as a more compact and stable absorption detection module will result in an improved temperature stability. This is especially important when AM-1f detection scheme is considered.

Finally, a simple arrangement of the sensor was evaluated, in which the gas exchange occurred only by diffusion, without forced gas flow. In that case, a response time $t_{10} = \sim$4.5 s (time required to reach 10% of the initial concentration) was obtained for a fully exposed spectrophone without any cell demonstrating that the QEPAS technique can deliver a response time in a few seconds range even without active gas flow. This is an important feature of the QEPAS technique in view of applications requiring an economical robust sensor platform with a fast response time.

References

1. A.A. Kosterev, Y.U. Bakhirkin, R.F. Curl, F.K. Tittel, Quartz-enhanced photoacoustic spectroscopy. Opt. Lett. **27**(21), 1902–1904 (2002)
2. A.A. Kosterev, F.K. Tittel, D.V. Serebryakov, A.L. Malinovsky, I.V. Morozov, Applications of quartz tuning forks in spectroscopic gas sensing. Rev. Sci. Instrum. **76**, 043105 (2005)
3. A.K.Y. Ngai, S.T. Persijni, D. Lindsay, A.A. Kosterev, P. Groß, C.J. Lee, S.M. Cristescu, F.K. Tittel, K.-J. Boller, F.J.M. Harren, Continuous wave optical parametric oscillator for quartz-enhanced photoacoustic trace gas sensing. Appl. Phys. B **89**, 123–128 (2007)
4. A.A. Kosterev, F.K. Tittel, Ammonia detection by use of quartz-enhanced photoacoustic spectroscopy with a near-IR telecommunication diode laser. Appl. Opt. **43**(33), 6213–6217 (2004)
5. G. Wysocki, A.A. Kosterev, F.K. Tittel, Influence of molecular relaxation dynamics on quartz-enhanced photoacoustic detection of CO_2 at $\lambda = 2$ μm. Appl. Phys. B **85**(2–3), 301–306 (2006)
6. A.A. Kosterev, T.S. Mosely, F.K. Tittel, Impact of humidity on quartz-enhanced photoacoustic spectroscopy based detection of HCN. Appl. Phys. B **85**(2–3), 295–300 (2006)
7. A.A. Kosterev, F.K. Tittel, QEPAS based detection of H_2S and CO_2 using a near-IR DFB diode laser, in *6th International Conference on Tunable Diode Laser Spectroscopy*, July 9–13, 2007, Reims, France
8. M.D. Wojcik, M.C. Phillips, B.D. Cannon, M.S. Taubman, Gas-phase photoacoustic sensor at 8.41 μm using quartz tuning forks and amplitude-modulated quantum cascade lasers. Appl. Phys. B **85**(2–3), 307–313 (2006)
9. M.C. Phillips, T.L. Myers, M.D. Wojcik, B.D. Cannon, External cavity quantum cascade laser for quartz tuning fork photoacoustic spectroscopy of broad absorption features. Opt. Lett. **32**(9), 1177–1179 (2006)
10. R. Lewicki, G. Wysocki, A.A. Kosterev, F.K. Tittel, QEPAS based detection of broadband absorbing molecules using a widely tunable, cw quantum cascade laser at 8.4 μm. Opt. Express **15**(12), 7357–7366 (2007)
11. P. Kluczynski, J. Gustafsson, Å.M. Lindberg, O. Axner, Wavelength modulation absorption spectrometry—an extensive scrutiny of the generation of signals. Spectrochim. Acta, Part B **56**, 1277–1354 (2001)

12. S. Schilt, L. Thévenaz, Ph. Robert, Wavelength modulation spectroscopy: combined frequency and intensity laser modulation. Appl. Opt. **42**, 6728–6738 (2003)
13. S.W. Sharpe, T.H. Johnson, R.L. Sams, P.M. Chu, G.C. Rhoderick, P.A. Johnson, Gas-phase database for quantitative infrared spectroscopy. Appl. Spectrosc. **58**, 1452–1461 (2004)
14. L.S. Rothman, D. Jacquemart, A. Barbe, D. Chris Benner, M. Birk, L.R. Brown, M.R. Carleer, C. Chackerian Jr., K. Chance, L.H. Coudert, V. Dana, V.M. Devi, J.-M. Flaud, R.R. Gamache, A. Goldman, J.-M. Hartmann, K.W. Jucks, A.G. Maki, J.-Y. Mandin, S.T. Massie, J. Orphal, A. Perrin, C.P. Rinsland, M.A.H. Smith, J. Tennyson, R.N. Tolchenov, R.A. Toth, J. Vander Auwera, P. Varanasi, G. Wagner, The HITRAN 2004 molecular spectroscopic database. J. Quantum Spectrosc. Radiat. Transf. **96**, 139–204 (2005)
15. A. Veres, Z. Bozóki, Á. Mohácsi, M. Szakáll, G. Szabó, External cavity diode laser based photoacoustic detection of CO_2 at 1.43 μm: the effect of molecular relaxation. Appl. Spectrosc. **57**, 900–905 (2003)
16. S. Schilt, J.-P. Besson, L. Thévenaz, Near-infrared laser photoacoustic detection of methane: the impact of molecular relaxation. Appl. Phys. B **82**(2), 319–328 (2006)
17. J.-P. Besson, S. Schilt, L. Thévenaz, Molecular relaxation effects on hydrogen chloride photoacoustic detection. Appl. Phys. B **90**(2), 191–196 (2008)
18. A.A. Kosterev, Y.A. Bakhirkin, F.K. Tittel, S. Blaser, Y. Bonetti, L. Hvozdara, Photoacoustic phase shift as a chemically selective spectroscopic parameter. Appl. Phys. B **78**, 673–676 (2004)
19. Y.L. Hoo, W. Jin, C. Shi, H.L. Ho, D.N. Wang, S.C. Ruan, Design and modeling of a photonic crystal fiber gas sensor. Appl. Opt. **42**(18), 3509–3515 (2003)
20. N. Gayraud, L.W. Kornaszewski, J.M. Stone, J.C. Knight, D.T. Reid, D.P. Hand, W.N. MacPherson, Mid-infrared gas sensing using a photonic bandgap fiber. Appl. Opt. **47**(9), 1269–1277 (2008)
21. S. Schilt, L. Thévenaz, Wavelength modulation photoacoustic spectroscopy: theoretical description and experimental results. Infrared Phys. Technol. **48**(2), 154–162 (2006)